

Novel seed-assisted synthesis of indium tin oxide submicro-cubes and their resistivity

Ting Liu, Zhucheng Jiang, Jiaxiang Liu (✉)

Beijing Key Laboratory of Electrochemical Process and Technology for Materials, College of Materials Science and Engineering, Beijing University of Chemical Technology, Beijing 100029, China

© Higher Education Press 2023

Abstract Indium tin oxide films, an important n-type semiconductor oxide, show great prospects in optoelectronic device applications. Consequently, as a key raw material of targets for sputtering films, it is important to prepare low-resistivity indium tin oxide powders. Herein, low-resistivity indium tin oxide submicro-cubes are synthesized by a seed-assisted coprecipitation method. The effects of seed content, In^{3+} concentration, aging time, reaction temperature and calcination temperature on resistivity were investigated by single factor and orthogonal experiments. To ensure reliability and reproducibility of data, each experiment was repeated three times and resistivity of each sample was measured three times to obtain average value. The results indicated that optimal sample was matched with cubic phase In_2O_3 . The single-crystal indium tin oxide particles exhibited a regular cubic shape with a size of nearly 500 nm and low resistivity of 0.814 $\Omega\cdot\text{cm}$. Compared with particles prepared by the conventional coprecipitation method, indium tin oxide submicro-cubes showed good dispersion. The presence of seed particles provided nucleation sites with lower energy barriers and promoted formation of submicro-cubes. The face-to-face contact among particles and good dispersion contributed to electron transfer, resulting in lower resistivity. The seed-assisted synthesis provides a novel way to prepare low-resistivity indium tin oxide submicro-cubes.

Keywords indium tin oxide, submicro-cubes, resistivity, seed-assisted coprecipitation method, orthogonal experiment

1 Introduction

In recent years, transparent conductive oxide films have

been widely explored owing to their potential applications in optoelectronic devices [1]. Indium tin oxide (ITO) films, as a representative transparent conducting oxide, have attracted increasing attention due to their excellent physical and chemical performance, including low resistivity, high optical transmittance, wide optical band gap and high infrared reflectance [2]. Based on the above performance, ITO films have been a desirable candidate for flat-panel displays [3], electrochromic devices [4], light-emitting diodes [5] and electrode materials [6]. It is worth mentioning that ITO films processed by annealing procedures are used as flexible low-cost substrates for materials such polyimide or paper [7,8]. At present, the mainstream industrial preparation method of ITO films is direct current magnetron sputtering and the properties of the films greatly depends on the quality of ITO targets [9]. Therefore, many aspects of ITO powders as important raw material of targets have been extensively investigated. Most studies focus on the preparation and performance of ITO powders [10], and it has been reported that the shape and resistivity of ITO powders have an influence on targets performance [11,12]. When ITO powders are cubic shape, the face-to-face contact between particles is beneficial to electron transfer [9]. Moreover, different forms of ITO particles with low-dimensional and quasi-one-dimensional structures, including nano-spheres [13], nano-rods [14], nano-wires [15] and nano-circles [16], are also important for optoelectronic device requiring large surface areas [17]. To the best of our knowledge, most scholars have focused on the preparation of ITO nano-spheres, but there have been a few studies on the preparation of ITO submicro-cubes. As a result, it is important to synthesize large-size cubic ITO powders with low resistivity.

To obtain ITO crystalline powders, many preparation methods have been proposed including hydrothermal synthesis [18], solvothermal process [19], sol-gel method [20] and microemulsion method [21]. Most of the mentioned methods remain challenges, requiring specific

apparatuses or complex synthetic routes. As a common powder preparation method, the chemical coprecipitation approach with simplicity and readily industrialization has been extensively utilized to synthesize ITO powders [22,23]. Seo et al. [22] obtained cubic and rhombohedral phase nanocrystalline ITO powders using ammonia as a precipitator at different reaction temperatures and aging time. Jafari et al. [23] synthesized cubic phase ITO nanoparticles by the coprecipitation method in the presence of surfactants of LABS and Triton X-100. Senthilkumar et al. [24] prepared cubic phase ITO nanopowders via a coprecipitation method in mixed solution of acetylacetone, methanol and water. In these studies, harsh condition and toxic organic solvents are required for the preparation of ITO powders, which are environmentally unfriendly. Moreover, the as-prepared powders have poor dispersion and serious particle agglomerates [22–24], which can deteriorate the density and resistivity of ITO targets. As a consequence, it is urgent to modify coprecipitation method for the preparation of ITO powders with low resistivity and good dispersion.

In this paper, the low-resistivity ITO submicro-cubes were synthesized via novel seed-assisted coprecipitation method. First, the effects of seed content, In^{3+} concentration, aging time, reaction temperature and calcination temperature on the resistivity and morphology of ITO powders were investigated by single factor experiment. Whereafter, on the basis of single factor experiment results, we found the optimum preparation process combination to obtain low-resistivity ITO powders under the guidance of orthogonal experiment. Then, the thermal decomposition process, activation energy, phase composition, morphology, microstructure and resistivity of optimal ITO submicro-cubes were characterized in detail. Finally, the synthesis mechanism of ITO submicro-cubes was analyzed. Compared with the existing ITO powders synthesized via the conventional coprecipitation method, as-prepared ITO submicro-cubes have advantages of an environmentally-friendly reaction regimen, low resistivity and good dispersion. This work provides a novel method to realize large-size and low-resistivity ITO powders. The ITO submicro-cubes with low resistivity have great application prospects in the preparation of ITO targets.

2 Experimental

2.1 Materials

Metal In (99.99%) was purchased from Liuzhou Smelting Co., Ltd. Indium nitrate ($\text{In}(\text{NO}_3)_3 \cdot 4\text{H}_2\text{O}$, 99.99%) and stannic chloride ($\text{SnCl}_4 \cdot 5\text{H}_2\text{O}$, 99.99%) were purchased from Macklin Biochemical Technology Co., Ltd. NaOH and urea were analytically pure and purchased from Beijing Tong Guang Fine Chemicals Co., Ltd.

2.2 Preparation of seed solution

First, 0.2708 g $\text{In}(\text{NO}_3)_3 \cdot 4\text{H}_2\text{O}$ and 0.0323 g $\text{SnCl}_4 \cdot 5\text{H}_2\text{O}$ were dissolved in deionized water (96 mL) to obtain a mixed salt solution. Under vigorous stirring, 4 mL NaOH solution ($c = 0.625 \text{ mol} \cdot \text{L}^{-1}$) was added dropwise into the above solution to adjust the pH to 4.0. Then, the mixed solution was stirred at room temperature for 6 h to obtain a slight-white transparent colloidal seed solution.

2.3 Preparation of ITO submicro-cubes

In this work, urea was used as the precipitant. Metal In (5.0 g) was dissolved in concentrated hydrochloric acid of 10 mL at 80 °C for subsequent experiment. The synthesis process of ITO submicro-cubes is illustrated in Fig. 1. First, under continuous stirring, the appropriate amount of as-prepared seed solution and urea were added into the freshly prepared mixed salt solution (i.e., In^{3+} and Sn^{4+}) at certain reaction temperatures. In the above mixed solution, the indium concentration (i.e., 0.02, 0.04, 0.06, 0.08 and 0.1 $\text{mol} \cdot \text{L}^{-1}$) was adjusted with hydrochloric acid containing In^{3+} and deionized water, the amount of $\text{SnCl}_4 \cdot 5\text{H}_2\text{O}$ was fixed according to a mass ratio of $m(\text{In}_2\text{O}_3):m(\text{SnO}_2) = 9:1$, where the amount of urea was designed according to molar ratio of $n(\text{urea}):n(\text{cation}) = 15:1$. The addition amount of as-prepared seed solution was determined in accordance with seed content in the final ITO powders. Herein, the seed contents were 0, 2, 4, 6 and 8 wt %, respectively. Subsequently, the above mixed salt solution was stirred at different reaction temperatures (i.e., 75, 80, 85 and 90 °C) for 2–10 h (i.e.,



Fig. 1 Schematic diagram of ITO submicro-cubes synthesis process.

2, 4, 6, 8 and 10 h). Then, the obtained white precipitate was centrifuged and washed five times with deionized water and ethanol, and dried at 60 °C for 4 h. Ultimately, the precursors were ground and calcined in a muffle furnace at different calcination temperatures (i.e., 600, 650, 700, 750 and 800 °C) for 2 h to obtain yellow ITO submicro-cubes.

2.4 Characterization

Thermogravimetric (TG) and differential scanning calorimetry (DSC) analyses of precursors were performed in a Mettler Toledo 2+ simultaneous thermal analyzer with a heating rate of 5, 10, 15 and 20 °C·min⁻¹. The phase composition of the samples was examined by X-ray powder diffraction (XRD, D8 Advance) using Cu K α radiation ($\lambda = 1.5418 \text{ \AA}$, 40 kV, 40 mA). The morphology and microstructure of powders were characterized by scanning electron microscopy (SEM, Zeiss Supra 55), high-resolution transmission electron microscopy (HRTEM, FEI Tecnai F30-ST) and energy-dispersive X-ray spectroscopy (EDS) coupled with HRTEM. To measure the electrical performance of ITO powders, ITO disks with 10 mm diameter and 2 mm thickness were prepared by die pressing under 5 MPa. The resistivity was recorded by four-point probes resistivity measurement system (RTS-9), and the resistivity of each sample was measured three times to obtain the average value. Carrier concentration and mobility were measured three times by a Hall effect measurement system (LanHai Instrument Co., Ltd.). Ultraviolet-visible spectrophotometer (UV-

Vis, Shimadzu UV-3600) was utilized to obtain the diffusion reflection spectra.

3 Results and discussion

3.1 Effects of preparation process on the resistivity and morphology

Resistivity is an important parameter to assess the properties of ITO powders [2]. To obtain low-resistivity ITO powders, single factor experiment was conducted and each experiment was repeated three times for reproducibility and accuracy. Figure 2 shows the effects of seed content, In³⁺ concentration, aging time, reaction temperature and calcination temperature on the resistivity of ITO powders. As shown in Fig. 2(a), the minimum resistivity of ITO powders occurred at seed content of 6 wt %. In this work, ITO powders were prepared by thermal dehydration of precursor particles, therefore the dispersion of precursor particles could affect that of ITO powders. Also, the larger grain size of precursor particles was, the larger grain size of ITO powders was. According to a previous study, the grain size is considered a significant factor that controls the resistivity of ITO powders [25]. This is because grain size can affect the number of grain boundary, namely, the larger the grain size is, the smaller the grain boundary number is, resulting in a reduced grain boundary scattering and improved electron mobility, thus the resistivity of ITO

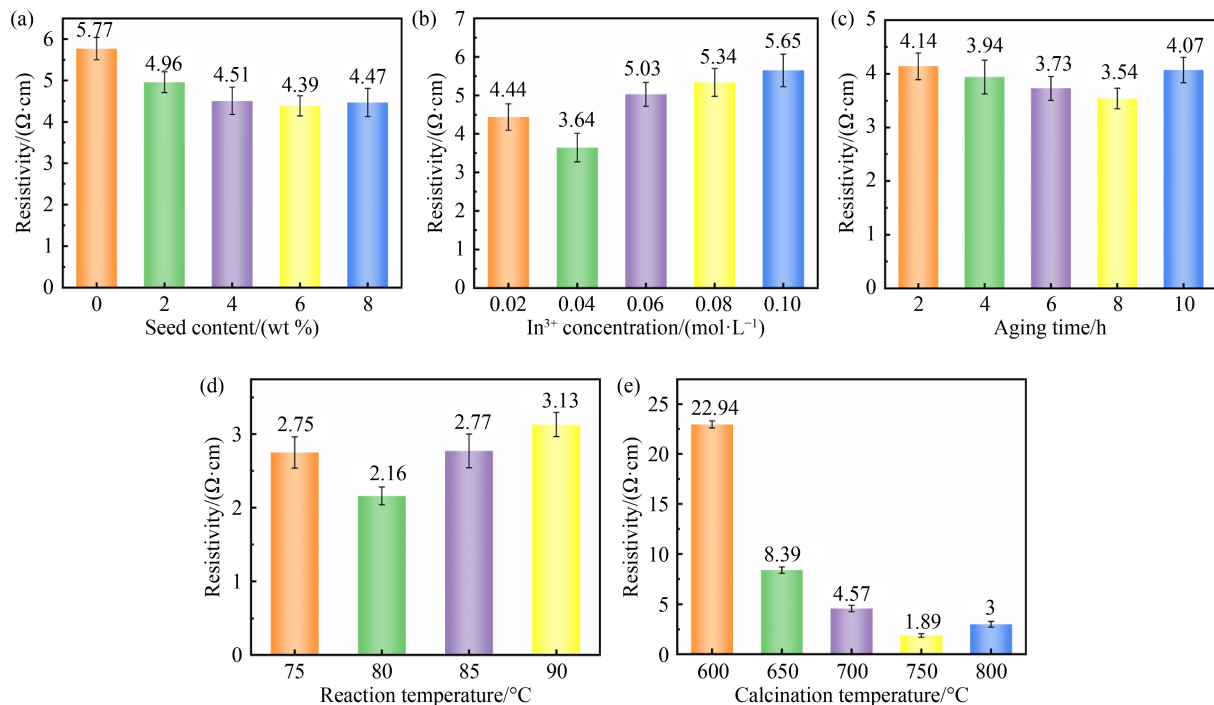


Fig. 2 Resistivity of ITO powders as a function of different factors: (a) seed content, (b) In³⁺ concentration, (c) aging time, (d) reaction temperature, and (e) calcination temperature.

powders decreased [26,27]. In mixed salt solution, the addition of seed particles composed of indium tin hydroxide promoted the crystallization of ITO precursor particles. The crystallinity and grain size of precursor particles increased with increasing seed content [28], which is beneficial to obtaining ITO powders with large grain size and thus decreasing the resistivity. In Fig. 2(b), the resistivity decreased first and then steadily rose with In^{3+} concentration increase and reached a minimum value at $0.04 \text{ mol}\cdot\text{L}^{-1}$. With In^{3+} concentration increasing, the amount of In^{3+} attaching to the surface of seed particles was increased, which led to the larger grain size of precursor particles. Unfortunately, excessive In^{3+} concentration caused serious agglomeration of powders. It has been reported that the poor dispersion of ITO powders could result in higher resistivity [29]. Figure 2(c) shows that the resistivity achieves the lowest value of $3.54 \text{ }\Omega\cdot\text{cm}$ at 8 h. Because the grain size of precursor particles could grow larger with prolonged aging time [30], the resistivity of ITO powders showed a downward trend. However, when aging time continued to increase, the single precursor particles were gathered together due to the collision between particles [31], which deteriorated the dispersion of precursor particles, leading to resistivity increase of ITO powders. Figure 2(d) shows that the resistivity reaches the lowest point at $80 \text{ }^\circ\text{C}$. The decomposition temperature of urea is $74 \text{ }^\circ\text{C}$ [32], and when the reaction temperature is higher than $74 \text{ }^\circ\text{C}$, OH^- and CO_2 can be generated in the solution [33]. The generation rate of OH^- increased with increasing reaction temperature, which promoted the increase in grain size of precursor particles [34]. However, when the reaction temperature was above $80 \text{ }^\circ\text{C}$, excessive generation of OH^- may cause inhomogeneous growth of precursor particles, resulting in the poor dispersion and high

resistivity of ITO powders. As shown in Fig. 2(e), the resistivity decreased first and then increased with increasing calcination temperature. It could be clearly observed that the resistivity was lowest at $750 \text{ }^\circ\text{C}$. It has been reported that rising calcination temperature can increase the grain size of ITO powders, which is beneficial for electron transfer and lower resistivity [12]. Nevertheless, when the calcination temperature was higher than $750 \text{ }^\circ\text{C}$, the dispersion of ITO powders became poor and hard agglomerates were formed [35], which increased the grain boundary scattering and resistivity of powders.

Based on above analysis regarding the effects of seed content, In^{3+} concentration, aging time, reaction temperature and calcination temperature on the resistivity of ITO powders, relatively better preparation process is obtained: seed content is 6 wt %, In^{3+} concentration is $0.04 \text{ mol}\cdot\text{L}^{-1}$, aging time is 8 h, reaction temperature is $80 \text{ }^\circ\text{C}$ and calcination temperature is $750 \text{ }^\circ\text{C}$. The minimum resistivity value reaches $1.89 \text{ }\Omega\cdot\text{cm}$ under relatively better preparation process.

To investigate the effect of calcination temperature on particle size and shape, which further influences the resistivity of ITO powders, SEM was used to observe the morphology. Figure 3 shows the SEM images of ITO powders prepared at different calcination temperatures. As shown in the figure, when the calcination temperature was lower than $700 \text{ }^\circ\text{C}$, the irregular-shaped ITO powders had poor dispersion and presented a large number of agglomerates consisting of smaller particles. With increasing calcination temperature to $700 \text{ }^\circ\text{C}$, the powders presented a cubic shape, but the particle size distribution was scattered. When the calcination temperature rose to $750 \text{ }^\circ\text{C}$, the ITO powders evidently became larger and exhibited a regular cubic shape with a size of

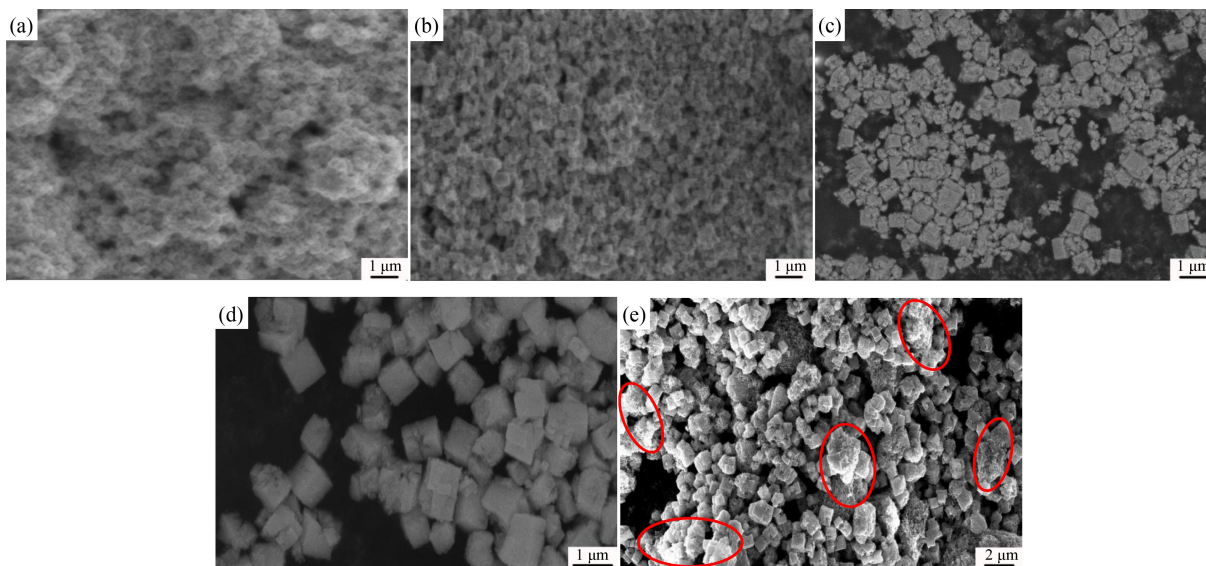


Fig. 3 SEM images of ITO powders prepared at different calcination temperatures: (a) $600 \text{ }^\circ\text{C}$, (b) $650 \text{ }^\circ\text{C}$, (c) $700 \text{ }^\circ\text{C}$, (d) $750 \text{ }^\circ\text{C}$, and (e) $800 \text{ }^\circ\text{C}$.

500–600 nm, and the powder dispersion improved. For ITO green bodies, taking ITO particle shape into consideration, the electrons could be easily transferred due to face-to-face contact between large-size cubic particles [19], which reduced the grain boundary scattering and was beneficial for lower resistivity. However, with further increases in calcination temperature to 800 °C, ITO particles with serious hard agglomerations became larger, and the particle agglomerations could severely deteriorate resistivity. According to the above analysis, the results of SEM analysis are consistent with the tendency of resistivity in Fig. 2(e).

3.2 Optimal ITO submicro-cubes preparation process by orthogonal experiment

3.2.1 Orthogonal experiment design and data

Although single factor experiment can explore the effect of every factor on resistivity, the optimal preparation process combination of ITO powders synthesized by a seed-assisted coprecipitation method cannot be obtained. Orthogonal experiment is a time-saving and economical approach to investigate multi-factor comprehensive effects by statistical mathematical analysis. Some representative points from the overall possible range are selected to conduct the experiments [36]. As a result, in this work, orthogonal experiment was adopted to further obtain the optimal preparation process combination of ITO powders with low resistivity. Based on the above single factor experimental results, four factors were selected for orthogonal experiment optimization: seed content, In³⁺ concentration, reaction temperature and calcination temperature, which had more prominent effects on the resistivity of ITO powders. The negligible interaction among the four factors was not considered, so an orthogonal array table L9(3⁴) was applied to design the orthogonal experiment [37]. Significantly, the experimental method ignoring the interaction among factors has been successfully used to explore the optimal preparation process combination of other inorganic materials [36,38,39]. Table 1 shows four factors and three levels of orthogonal experiment, and Table 2 lists the plan and results of orthogonal experiment. Herein, each sample was synthesized two times under the same preparation process combination to ensure the reproducibility, where R_{ik} is the average value of measured resistivity.

Table 1 Factors and levels of orthogonal experiment design

Level	Factor			
	Seed content/ wt % (A)	In ³⁺ concentration/ (mol·L ⁻¹) (B)	Reaction temperature/ °C (C)	Calcination temperature/ °C (D)
I	2	0.04	75	650
II	4	0.06	80	700
III	6	0.08	85	750

3.2.2 Range analysis of the orthogonal experiment results

According to the results in Table 2, the optimal preparation process combination could not be acquired. Because the range analysis could qualitatively show the significance degree of each factor on resistivity by comparing range values and obtain the best process combination, range analysis was adopted to analyze the results. \bar{K}_{1j} , \bar{K}_{2j} , \bar{K}_{3j} and R are four important values in range analysis, and they are defined as the average resistivity of three levels for each factor j ($j = A, B, C, D$) and the difference between the maximum and minimum value of \bar{K}_{1j} , \bar{K}_{2j} , \bar{K}_{3j} , namely $R = \bar{K}_{\max} - \bar{K}_{\min}$. A larger R value means that the factor has a greater effect on the resistivity of ITO powders. Table 3 shows all orthogonal experimental results and calculation results of range analysis. For factor A, the average resistivity of I level is maximal (9.96), and the average resistivity of III level is minimal (5.68), so the R value of factor A is 4.28. In the same way, the R values of factors B, C and D can be obtained. As shown in Table 3, the values of R_A , R_B , R_C and R_D are 4.28, 2.40, 2.53 and 6.82, respectively, indicating that the effect of calcination temperature on the resistivity of ITO powders is the largest, followed by seed content, reaction temperature and In³⁺ concentration. Based on above results, the best preparation process

Table 2 Orthogonal experiment design and results

No.	Factor				Resistivity $R_{ik}/(\Omega \cdot \text{cm})$	
	A	B	C	D	1	2
1	2	0.04	75	650	14.27	15.39
2	2	0.06	80	700	8.98	9.72
3	2	0.08	85	750	5.86	5.54
4	4	0.04	80	750	4.89	4.58
5	4	0.06	85	650	9.93	9.69
6	4	0.08	75	700	13.63	12.57
7	6	0.04	85	700	8.02	8.25
8	6	0.06	75	750	1.11	1.54
9	6	0.08	80	650	8.08	7.07

Table 3 Range analysis of orthogonal experiment data

No.	Factor				Resistivity $R_{ik}/(\Omega \cdot \text{cm})$	
	A	B	C	D	1	2
1	2	0.04	75	650	14.27	15.39
2	2	0.06	80	700	8.98	9.72
3	2	0.08	85	750	5.86	5.54
4	4	0.04	80	750	4.89	4.58
5	4	0.06	85	650	9.93	9.69
6	4	0.08	75	700	13.63	12.57
7	6	0.04	85	700	8.02	8.25
8	6	0.06	75	750	1.11	1.54
9	6	0.08	80	650	8.08	7.07
\bar{K}_{1j}	9.96	9.23	9.75	10.74		
\bar{K}_{2j}	9.22	6.83	7.22	10.20		
\bar{K}_{3j}	5.68	8.79	7.88	3.92		
R	4.28	2.40	2.53	6.82		

combination is $A_3B_2C_2D_3$; seed content is 6 wt %, In^{3+} concentration is $0.06 \text{ mol}\cdot\text{L}^{-1}$, reaction temperature is $80 \text{ }^\circ\text{C}$ and calcination temperature is $750 \text{ }^\circ\text{C}$.

3.2.3 Variance analysis of the orthogonal experiment results

Although range analysis could give the significance degree of each factor and the best preparation process combination, the experimental error magnitude could not be obtained [36]. The variance analysis not only gives data fluctuation for each factor leading to experimental error, but also verifies the significance order obtained by range analysis [38]. It is worth noting that F value is an important parameter in variance analysis, which could quantitatively evaluate the significance degree of each factor. F_α is a constant value and could be found from the distribution table of F -value [36,38,39]. By comparing the calculated F_j value with F_α ($\alpha = 0.01, 0.05$), the factor effect on experimental results is obtained. All orthogonal experimental results and calculation results of variance analysis are listed in Table 4. For variance analysis of factor A, we could follow the below calculation process. The sum of squared deviation for factor A (S_A) is:

$$S_A = \sum_{h=1}^3 n_h (\bar{R}_h - \bar{R})^2 = 62.79141, \quad (1)$$

where n_h is experimental times at the same level of factor A, \bar{R}_h is average resistivity at the same level of factor A, and \bar{R} is average resistivity of all test data. The freedom degree of factor A (f_A) is:

$$f_A = 3 - 1 = 2. \quad (2)$$

The sum of squared deviation generated by repeated experimental error (S_e) is:

$$S_e = \sum_{i=1}^9 \sum_{k=1}^2 (R_{ik} - \bar{R}_i)^2 = 2.21980, \quad (3)$$

Table 4 Variance analysis of orthogonal experiment data

No.	Factor				Resistivity $R_{ik}/(\Omega\cdot\text{cm})$	
	A	B	C	D	1	2
1	2	0.04	75	650	14.27	15.39
2	2	0.06	80	700	8.98	9.72
3	2	0.08	85	750	5.86	5.54
4	4	0.04	80	750	4.89	4.58
5	4	0.06	85	650	9.93	9.69
6	4	0.08	75	700	13.63	12.57
7	6	0.04	85	700	8.02	8.25
8	6	0.06	75	750	1.11	1.54
9	6	0.08	80	650	8.08	7.07
S_j	62.79141	19.66754	20.68808	172.32100	$S_e = 2.21980$	
f_j	2	2	2	2	$f_e = 9$	
F_j	127.29140	39.87024	41.93907	349.33080	$F_{0.01}(2,9) = 8.02$	
					$F_{0.05}(2,9) = 4.26$	

where R_{ik} is measured resistivity of each group experiment and \bar{R}_i is average resistivity of each group experiment. The freedom degree of experimental error (f_e) is:

$$f_e = f_T - \sum f_j = (9 \times 2 - 1) - 4 \times 2 = 9, \quad (4)$$

F value of factor A is:

$$F_A = \frac{S_A/f_A}{S_e/f_e} = \frac{62.79141/2}{2.21980/9} = 127.29140. \quad (5)$$

In the same way, the sum of squared deviations S_B , S_C and S_D , the freedom degrees f_B , f_C and f_D , and the F values F_B , F_C and F_D are calculated by the above method. As shown in Table 4, the effects of calcination temperature (factor D), seed content (factor A), reaction temperature (factor C) and In^{3+} concentration (factor B) on the resistivity of ITO powders are prominent ($F_D > F_A > F_C > F_B > F_{0.01}$). The results of variance analysis correspond to those of range analysis, which means that the factor effect sequence on resistivity as follows: calcination temperature > seed content > reaction temperature > In^{3+} concentration.

3.3 Characterization of optimal ITO submicro-cubes

To confirm the best process combination obtained by orthogonal experiment, three times repeated experiments were conducted to synthesize the ITO submicro-cubes under the optimal preparation process combination, and the sample was characterized systematically. Figure 4 presents the phase composition of the optimum sample and thermal decomposition of precursors. The XRD pattern of precursor and as-prepared sample synthesized under the optimal preparation process is shown in Fig. 4(a). It could be seen that all diffraction peaks of the precursor corresponded well with those of the cubic phase $In(OH)_3$ (JCPDS No. 73-1810), and there were no other impurity phases. When $In(OH)_3$ precursors were calcined at $750 \text{ }^\circ\text{C}$ for 2 h, $In(OH)_3$ completely transformed to the cubic phase In_2O_3 (JCPDS No. 06-0416). No traces of any secondary phase could be seen in the XRD pattern, indicating that Sn^{4+} was completely incorporated into the main lattice of In_2O_3 . The sharp diffraction peaks of (222), (400), (440) and (622) demonstrated the high crystallinity of as-prepared ITO powders. Figure 4(b) displays the TG-DSC curves (at $20 \text{ }^\circ\text{C}\cdot\text{min}^{-1}$ heating rate) of the precursors, showing three mass loss stages. The first mass loss observed at low temperature (before $100 \text{ }^\circ\text{C}$) was attributed to the evaporation of ethanol and surface water. The second mass loss from 100 to $600 \text{ }^\circ\text{C}$ could be assigned to thermal dehydration from hydroxide precursor to oxide, accompanied with a weak endothermic peak at $288 \text{ }^\circ\text{C}$ [40]. This decomposition process resulted in an experimental mass loss value of 16.29%, which was close to theoretical mass loss value of 16.28% caused by the dehydration in $2In(OH)_3 \rightarrow In_2O_3 + 3H_2O(g)$ [41]. The TG-DSC data agreed well with the XRD pattern, which

also demonstrated the formation of $\text{In}(\text{OH})_3$ precursors. No further mass loss was observed above 600 °C in the TG curve, suggesting that the ITO phase was completely formed.

The thermal decomposition process of solids has been the focus of many kinetics studies. In the seed-assisted coprecipitation synthesis of ITO powders, indium tin hydroxide precursors as the intermediate can be decomposed by high-temperature calcination. In addition, the TG curve was very sharp (see Fig. 4(b)), indicating that the thermal decomposition process quickly took place [42]. As a result, it is essential to thoroughly know the energy requirement in calcination process of precursors. However, to the best of our knowledge, there have been few reports on the thermodynamic behavior of indium tin hydroxide decomposition. Figure 5 shows the thermal analysis kinetics of the indium tin hydroxide precursor. The activation energy in decomposition process was investigated using the TG technique (Fig. 5(a)). The activation energies for different conversions are calculated by the Flynn–Wall–Ozawa (FWO) method, which is useful for the complex decomposition reaction. The FWO equation is as follows [43]:

$$\lg \beta = \lg \left(\frac{AE}{RG(\alpha)} \right) - 2.315 - 0.4567 \frac{E}{RT}, \quad (6)$$

where β is heating rate ($\text{K} \cdot \text{min}^{-1}$), A is the pre-exponential factor, E is the activation energy ($\text{kJ} \cdot \text{mol}^{-1}$), R is the gas constant ($8.3145 \text{ J} \cdot \text{mol}^{-1} \cdot \text{K}^{-1}$), $G(\alpha)$ is the mechanism function, α is the degree of decomposition (%), T is the absolute temperature (K). The activation energy for different conversions can be calculated according to the slope of line derived by the linear fitting relationship of $\lg \beta$ versus $1/T$ (Fig. 5(b)). As shown in Fig. 5(c), the activation energy is dependent on conversion degree, and the activation energy of thermal decomposition process changed with different conversions. The average activation energy of decomposition process was $164.085 \text{ kJ} \cdot \text{mol}^{-1}$. These results show that the dehydration decomposition of indium tin hydroxide precursors is a multi-step kinetic reaction process.

The detailed morphology and microstructure are presented in Fig. 6. Figure 6(a) shows approximately 500 nm, well-dispersed and cubic-shaped ITO powders. The result was close to the observation obtained in Fig. 3(d). The HRTEM image of ITO powders presented that the measured lattice spacing value (0.25 nm) corresponded with the typical d-spacing of (400) lattice plane attributed to cubic phase In_2O_3 (Fig. 6(b)). Due to the incorporation of Sn^{4+} into In_2O_3 lattice, the measured lattice spacing was a little lower than the standard value of 0.2529 nm (JCPDS No. 06-0416) [44]. As shown in

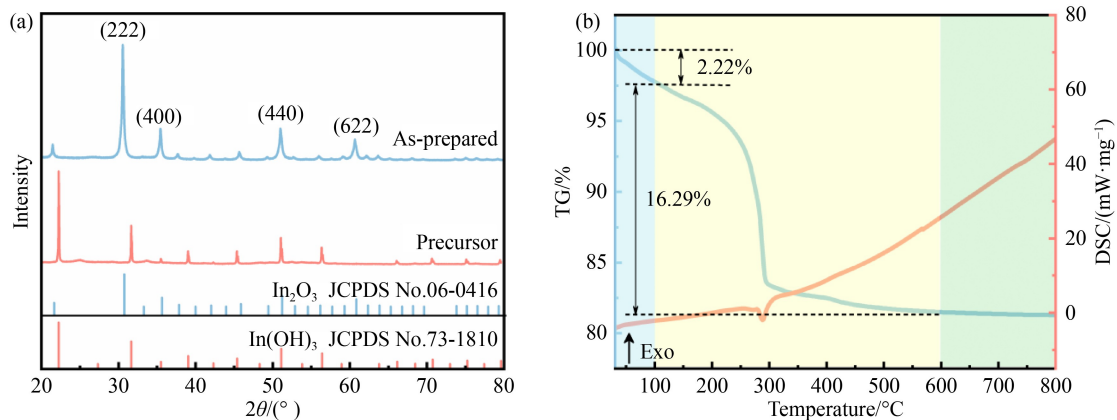


Fig. 4 The phase composition of the optimum sample and thermal decomposition of precursors: (a) XRD pattern, (b) TG-DSC curves of precursors.

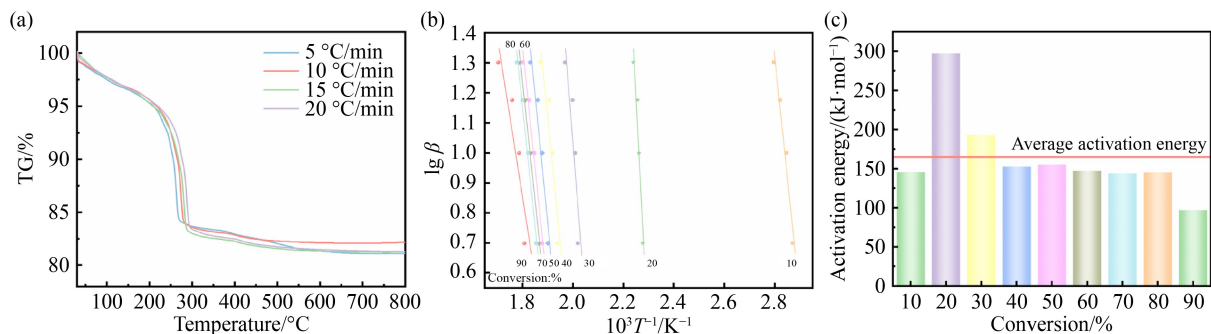


Fig. 5 Kinetic analysis of precursors: (a) TG curves of precursor powders at different heating rates, (b) linear fitting relationship of $\lg \beta$ versus $1/T$ corresponding to different conversions, and (c) activation energies at different conversions.

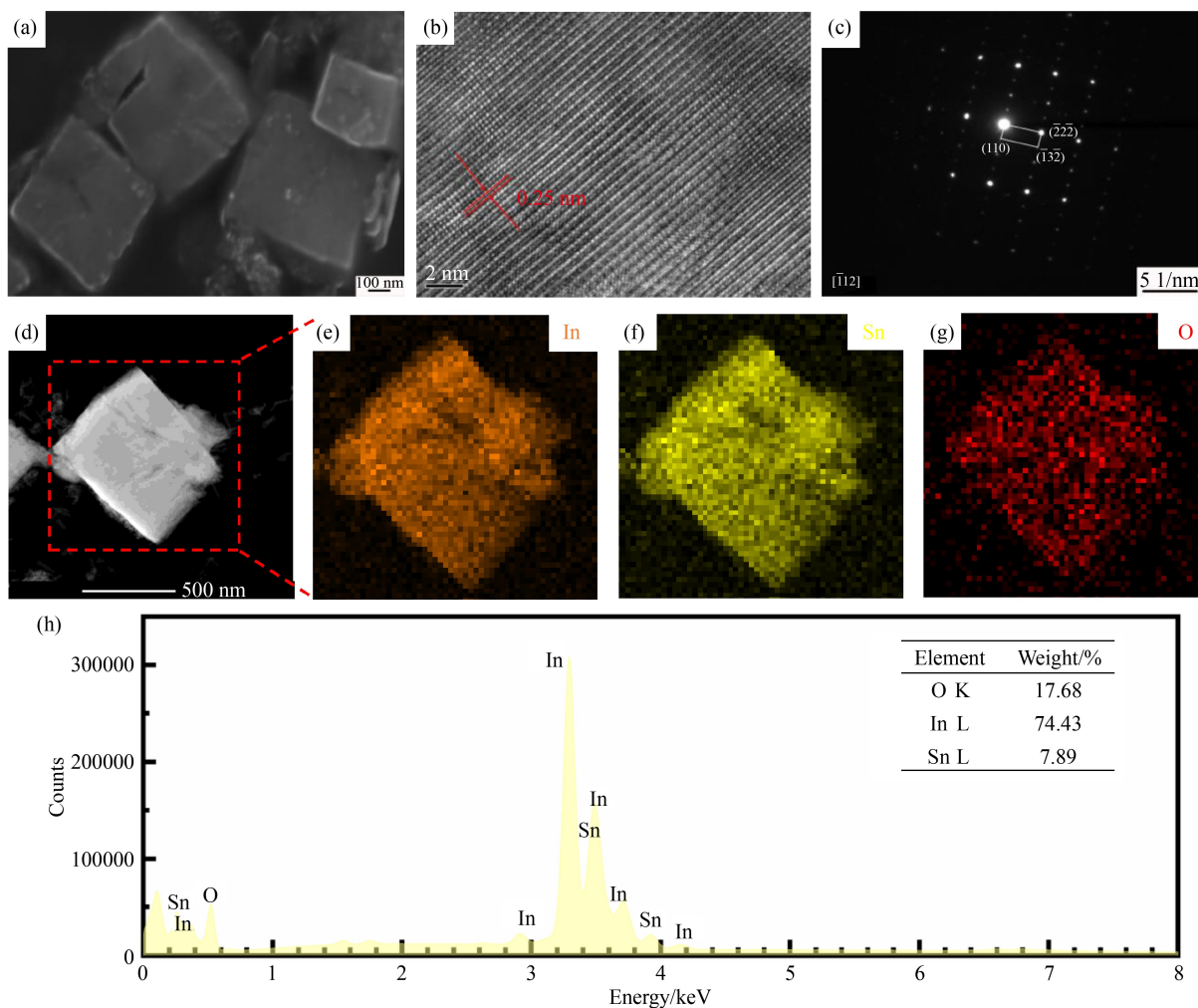


Fig. 6 The morphology and microstructure of ITO powders: (a) SEM image, (b) HRTEM image showing (400) plane with d-spacing of 0.25 nm, (c) SAED pattern, (d) HAADF-STEM image, EDS elemental mapping images of (e) In, (f) Sn, and (g) O, (h) EDS spectrum.

Fig. 6(c), the as-prepared ITO powders exhibited a highly-ordered single crystalline structure. The diffraction spots agreed well with the $(\bar{2}\bar{2}\bar{2})$, (110) and $(\bar{1}\bar{3}\bar{2})$ planes of cubic phase In_2O_3 without any diffraction spots of other oxides, which was the same as that reported in previous study [45] and further confirmed to as-prepared ITO powders with single cubic phase structure. The high-angle annular dark-field scanning transmission electron microscopy (HAADF-STEM) measurement was used to analyze the elemental distribution of ITO powders. As displayed in Figs. 6(d–g), three representative In, Sn, and O mappings indicate that the elements all had homogeneous distributions in single ITO grain. EDS spectrum was used to measure the elemental content of as-prepared ITO powders. Figure 6(h) presents that the mass ratio of In and Sn is 9.43:1, which agrees with the experimental additions.

Hall effect measurement was applied to obtain a detailed understanding of the electrical conductivity of as-prepared ITO powders. Figure 7 shows the electrical conductivity and comparison of the resistivity. The

column chart of resistivity, carrier concentration, and mobility is displayed in Fig. 7(a). ITO powders showed a resistivity of $0.814 \Omega \cdot \text{cm}$, carrier concentration of $2.52 \times 10^{15} \text{ cm}^{-3}$ and mobility of $3.05 \times 10^3 \text{ cm}^2 \cdot \text{V}^{-1} \cdot \text{s}^{-1}$. The resistivity of as-prepared ITO powders was comparable to or lower than those reported in the literature [2,22,24,34,46–48], as shown in Fig. 7(b). Because the large-size ITO powders showed cubic shape and good dispersion (see Figs. 3(d) and 6(a)), the contact area among particles was increased by press molding. It has been reported that the face-to-face contact among cubic particles contributes to electron transfer [9,19] and the good dispersion of powders is conducive to decreasing resistivity [29], so the as-prepared ITO powders showed high electron mobility and low resistivity. Furthermore, the carrier concentration had considerable effect on the optical band gap of ITO [49], therefore the band gap of as-prepared ITO powders was obtained by UV-Vis diffusion reflection spectra. Figure 7(c) shows the typical diffusion reflection spectra, and a corresponding absorption spectra of ITO powders was exhibited in the

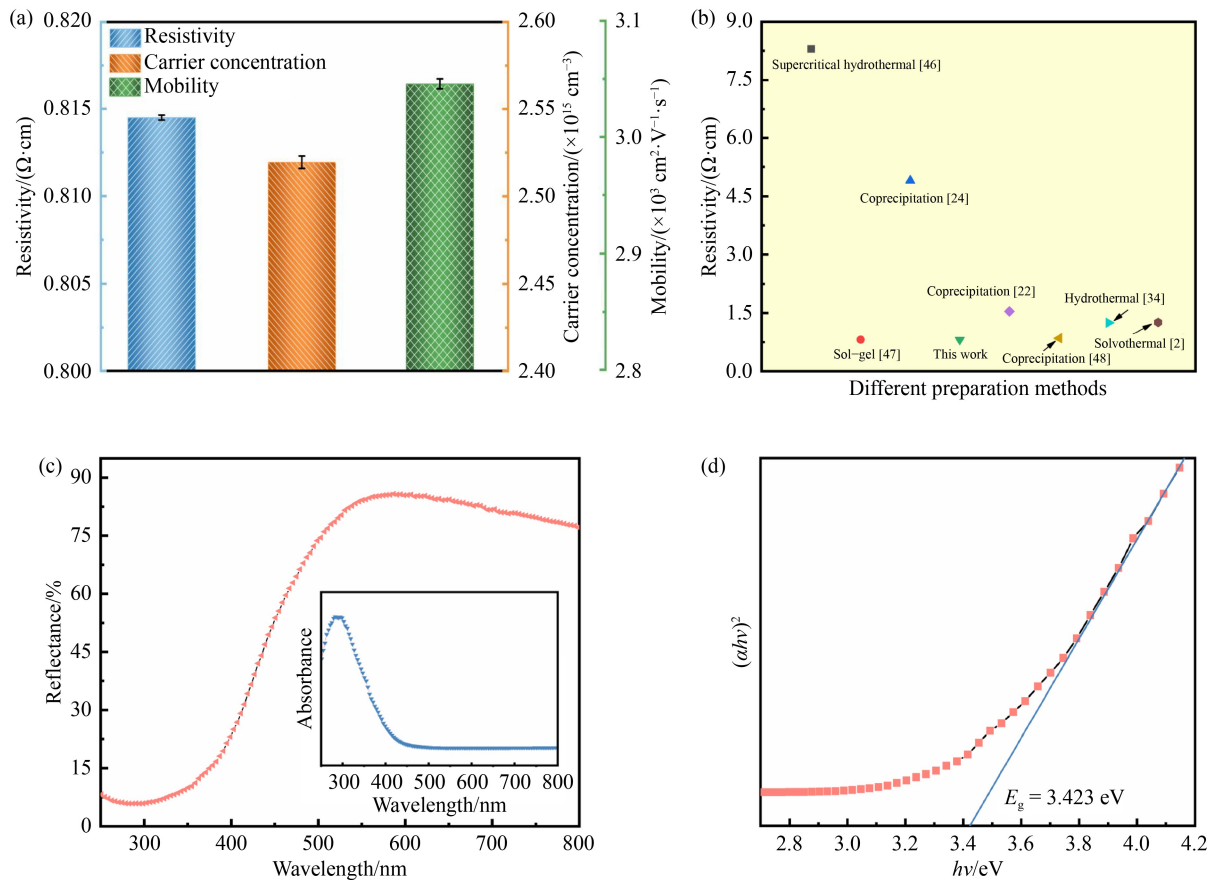


Fig. 7 (a) Column chart of resistivity, carrier concentration and mobility; (b) comparison of the resistivity for different preparation methods; (c) UV–Vis diffusion reflection spectra (insert of absorption spectra); (d) plot of $(\alpha hv)^2$ as function of hv .

insert according to Kubelka–Munk relationship. The band gap value obeys the following equation [50]:

$$(\alpha hv)^2 = A(hv - E_g). \quad (7)$$

Here, α is the absorption coefficient, hv is the photon energy, A is the constant restricted by the valence and conduction band of material, and E_g is the optical band gap. By linearly fitting on the edge of the corresponding curve, the intersection of the straight linear region on the hv axis of the plot of $(\alpha hv)^2$ versus hv provides the E_g . As shown in Fig. 7(d), the E_g value of 3.423 eV was slightly lower than that of intrinsic material (3.75 eV) [51] and comparable to that reported in the literature [52]. The difference in band gap may be related to the Sn doping and defect of oxygen deficiency [52].

3.4 Synthesis mechanism of ITO submicro-cubes

Based on above results and analysis, the seed-assisted coprecipitation synthesis is a promising method for the preparation of large-size cubic-shaped ITO powders. Therefore, the seed-assisted coprecipitation synthesis mechanism of ITO powders is worthy of further exploration. Figure 8 illustrates the schematic diagram for the synthesis mechanism of large-size cubic precursor

particles. The seed-assisted coprecipitation method takes advantage of the seed particles with low energy barriers, where the metal ions (i.e., In^{3+} and Sn^{4+}) and OH^- can preferentially attach to the surfaces of seed particles and grow into large-size indium tin hydroxide precursor particles.

Figure 9 shows the morphology of seed particles and precursor particles. First, the low-concentration indium tin hydroxide seed solution was prepared by the conventional coprecipitation method with $\text{In}(\text{NO}_3)_3$, SnCl_4 and NaOH as starting materials. The seed particles show a quasi-cubic shape with estimated particle size of 50 nm (Fig. 9(a)). Normally, under heating condition, the urea gradually decomposes to generate OH^- (Eq. (8)) [33], which causes free metal ions to directly form indium tin hydroxide precursors in the solution. However, due to the presence of seed particles, the free metal ions and OH^- can preferentially attach to the surfaces of seed particles to further generate hydroxide precursor. That is attributed to seed particles with the same chemical composition exhibiting lower energy barriers for nucleation and thus promoting the formation and crystallization of indium tin hydroxide [53]. Subsequently, the epitaxial growth of precursor particles on the center quasi-cubic seed particles occurs under

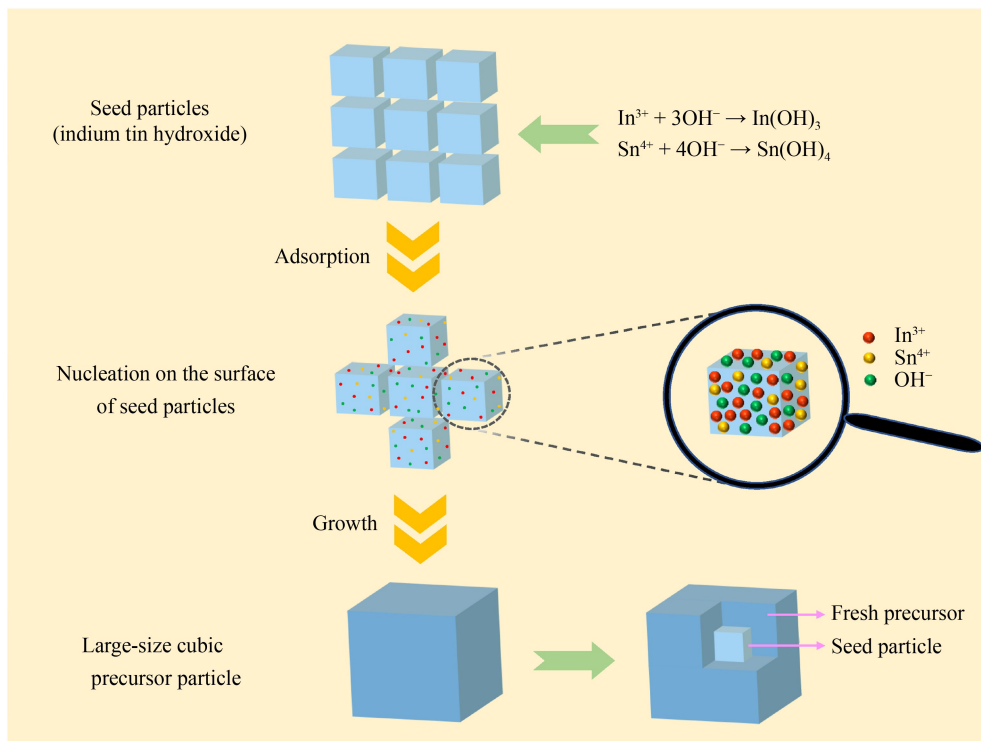


Fig. 8 Schematic illustration of the formation mechanism of large-size cubic precursor particles.

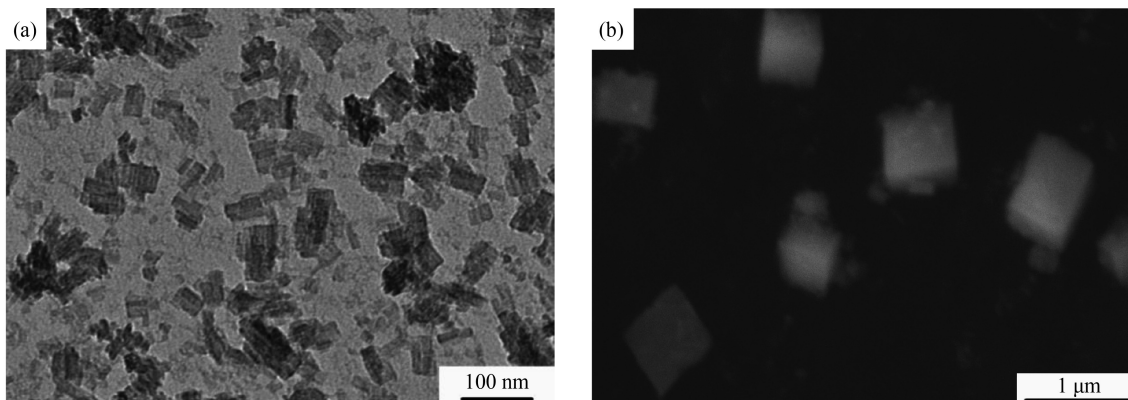


Fig. 9 The morphology of seed particles and precursor particles: (a) seed particles (TEM); (b) precursor particles (SEM).

heating condition [54], which results in the formation of large-size cubic precursor particles. Figure 9(b) presents the SEM image of indium tin precursor particles, in which the seed particles are contained and the particle morphology is shown to be nearly cubic-like. It has been reported that the shape of precursor particles could be controlled by the synthesis temperature without templates, in other words, the cubic-shaped indium tin hydroxide particles are easily formed at 80 °C [55]. Finally, the precursor particles dehydrate to generate ITO powders at high calcination temperature, and ITO powders inherit the shape of precursor particles (see Fig. 6(a)), which has been reported in the literature [55].



4 Conclusions

In this work, low-resistivity ITO submicro-cubes were synthesized by a simple seed-assisted coprecipitation method. Each single factor experiment was conducted three times for reliability and reproducibility, and the resistivity of each sample was measured three times to obtain the average value. Based on the results of single factor experiment, four factors with prominent influence, including seed content, In^{3+} concentration, reaction temperature and calcination temperature, were chosen for further orthogonal experiment optimization. Optimal preparation process combination was obtained: seed content was 6 wt %, In^{3+} concentration was $0.06 \text{ mol}\cdot\text{L}^{-1}$, reaction temperature was 80 °C, and calcination

temperature was 750 °C. The results showed that the average activation energy of decomposition ITO precursors was 164.085 kJ·mol⁻¹. The optimal and well-dispersed powders were indexed to cubic phase In₂O₃ and presented a cubic shape with a size of nearly 500 nm and low resistivity of 0.814 Ω·cm. The preparation process and the performance of sample had good reproducibility and reliability. The synthesis mechanism of ITO submicro-cubes was also systematically analyzed. The seed-assisted coprecipitation method took advantage of the seed particles with low energy barriers, the metal ions (i.e., In³⁺ and Sn⁴⁺) and OH⁻ could preferentially attach to the surfaces of seed particles, thus promoting epitaxial growth of large-size precursor particles and formation of ITO submicro-cubes. Notably, the face-to-face contact among particles and good dispersion were found to play major roles in electron transfer, which led to the low resistivity of ITO submicro-cubes. Compared with the traditional coprecipitation method, this strategy is a valuable approach for the preparation of low-resistivity and large-size ITO particles. The resultant ITO submicro-cubes could be used to prepare high-performance ITO targets to film sputtering.

Acknowledgements This work was financially supported by Beijing Natural Science Foundation (Grant No. 2192041).

References

- Medvedovski E, Alvarez N A, Szepesi C J, Yankov O, Lippens P. Advanced indium tin oxide ceramic sputtering targets (rotary and planar) for transparent conductive nanosized films. *Advances in Applied Ceramics*, 2013, 112(5): 243–256
- Ma Y, Zhai X, Liu J. Synthesis of hexagonal-phase indium tin oxide nanoparticles by deionized water and glycerol binary solvothermal method and their resistivity. *Journal of Materials Science*, 2020, 55(9): 3860–3870
- Mei F, Yuan T, Li R, Qin K, Zhou L, Wang W. Micro-structure of ITO ceramics sintered at different temperatures and its effect on the properties of deposited ITO films. *Journal of the European Ceramic Society*, 2018, 38(2): 521–533
- Song X, Dong G, Gao F, Xiao Y, Liu Q, Diao X. Properties of NiO_x and its influence upon all-thin-film ITO/NiO_x/LiTaO₃/WO₃/ITO electrochromic devices prepared by magnetron sputtering. *Vacuum*, 2015, 111: 48–54
- Sun C, Cheng C H, Zhang B L, Li R X, Wang Y, Liu W F, Luo Y M, Du G T, Cong S L. Green and low-cost approach to modify the indium tin oxide anodes in organic light-emitting diodes by electrochemical treatment in NaCl aqueous solution. *Applied Surface Science*, 2017, 422: 125–129
- Li L, Wang M, Fang Y, Qiao S. Investigation of electrochemical degradation and application of e-paper dyes in organic solvents. *Frontiers of Chemical Science and Engineering*, 2009, 3(2): 182–185
- Canhola P, Martins N, Raniero L, Pereira S, Fortunato E, Ferreira I, Martins R. Role of annealing environment on the performances of large area ITO films produced by rf magnetron sputtering. *Thin Solid Films*, 2005, 487(1–2): 271–276
- Baía I, Quintela M, Mendes L, Nunes P, Martins R. Performances exhibited by large area ITO layers produced by r.f. magnetron sputtering. *Thin Solid Films*, 1999, 337(1–2): 171–175
- Chen Y, Zhai X, Liu J. One-step solvothermal synthesis of cubic ITO nanopowders. *Rare Metal Materials and Engineering*, 2019, 48(7): 2358–2363 (in Chinese)
- Saito Y, Matsuno T, Guo Q, Mori T, Kashiwagi M, Shimojima A, Wada H, Kuroda K. Preparation of ordered nanoporous indium tin oxides with large crystallites and individual control over their thermal and electrical conductivities. *ACS Applied Materials & Interfaces*, 2021, 13(13): 15373–15382
- Zhai X, Chen Y, Ma Y, Liu Y, Liu J. Fabrication of monodisperse ITO submicro-spheres using L-Histidine-assisted one-step solvothermal method. *Ceramics International*, 2019, 45(14): 17562–17566
- Liu T, Zhai X, Liu J. Optimum preparation of low-resistivity indium tin oxide nanopowders via polyacrylamide gel route using orthogonal experiment. *Journal of Materials Science Materials in Electronics*, 2021, 32(17): 22232–22244
- Aziz M A, Zahir M H, Shaikh M N, Al-Betar A R, Oyama M, Sulaiman K O. Hydrothermal synthesis of tin-doped indium oxide nanoparticles using pamoic acid as an organic additive and their photoluminescence properties. *Journal of Materials Science Materials in Electronics*, 2017, 28(4): 3226–3233
- Pan K Y, Lin L D, Chang L W, Shih H C. Studies on the optoelectronic properties of the thermally evaporated tin-doped indium oxide nanostructures. *Applied Surface Science*, 2013, 273: 12–18
- Li L, Chen S, Kim J, Xu C, Zhao Y, Ziegler K J. Controlled synthesis of tin-doped indium oxide (ITO) nanowires. *Journal of Crystal Growth*, 2015, 413: 31–36
- Patel N G, Patel P D, Vaishnav V S. Indium tin oxide (ITO) thin film gas sensor for detection of methanol at room temperature. *Sensors and Actuators B: Chemical*, 2003, 96(1–2): 180–189
- Ayeshamariam A, Kashif M, Bououdina M, Hashim U, Jayachandran M, Ali M E. Morphological, structural, and gas-sensing characterization of tin-doped indium oxide nanoparticles. *Ceramics International*, 2014, 40(1): 1321–1328
- Wang H W, Xu G D, Zhang J R, Yin X. Hydrothermal synthesis of indium tin oxide nanoparticles without chlorine contamination. *Bulletin of the Korean Chemical Society*, 2014, 35(7): 1999–2003
- Sasaki T, Endo Y, Nakaya M, Kanie K, Nagatomi A, Tanoue K, Nakamura R, Muramatsu A. One-step solvothermal synthesis of cubic-shaped ITO nanoparticles precisely controlled in size and shape and their electrical resistivity. *Journal of Materials Chemistry*, 2010, 20(37): 8153–8157
- Bouzidi A, Omri K, Mir L E, Guermazi H. Preparation, structural and optical investigations of ITO nanopowder and ITO/epoxy nanocomposites. *Materials Science in Semiconductor Processing*, 2015, 39: 536–543
- Jiang Z, Liu T, Zhai X, Liu J. Optimization preparation of indium tin oxide nanoparticles via microemulsion method using orthogonal experiment. *Crystals*, 2021, 11(11): 1387

22. Seo K H, Lee J H, Kim J J, Bertoni M I, Ingram B J, Mason T O. Synthesis and electrical characterization of the polymorphic indium tin oxide nanocrystalline powders. *Journal of the American Ceramic Society*, 2006, 89(11): 3431–3436
23. Jafari A, Ganjkanlou Y, Kazemzad M, Ghorbani H. Effect of surfactants on the size, color, photoluminescence and resistivity of indium tin oxide nanoparticles prepared by co-precipitation method. *Surface Review and Letters*, 2012, 19(5): 1250054
24. Senthilkumar V, Senthil K, Vickraman P. Microstructural, electrical and optical properties of indium tin oxide (ITO) nanoparticles synthesized by co-precipitation method. *Materials Research Bulletin*, 2012, 47(4): 1051–1056
25. Ahmed N M, Sabah F A, Abdulgafour H I, Alsadig A, Sulieman A, Alkhoaaryef M. The effect of post annealing temperature on grain size of indium-tin-oxide for optical and electrical properties improvement. *Results in Physics*, 2019, 13: 102159
26. Lee J H, Kim Y H, Ahn S J, Ha T H, Kim H S. Grain-size effect on the electrical properties of nanocrystalline indium tin oxide thin films. *Materials Science and Engineering B*, 2015, 199: 37–41
27. Boehme M, Charton C. Properties of ITO on PET film in dependence on the coating conditions and thermal processing. *Surface and Coatings Technology*, 2005, 200(1–4): 932–935
28. Kobayashi Y, Mabuchi Y, Hama M, Inoue K, Yasuda Y, Morita T. Seeding technique for lowering temperature during synthesis of α -alumina. *Journal of Asian Ceramic Societies*, 2015, 3(1): 139–143
29. Ma Y, Liang F, Liu Y, Zhai X, Liu J. Effect of dispersion on visible light transmittance and resistivity of indium tin oxide nanoparticles prepared by cetyltrimethylammonium bromide-assisted coprecipitation method. *Journal of Materials Science Materials in Electronics*, 2019, 30(19): 17963–17971
30. Jalilpour M, Fathalilou M. Effect of aging time and calcination temperature on the cerium oxide nanoparticles synthesis via reverse co-precipitation method. *International Journal of Physical Sciences*, 2012, 7(6): 944–948
31. Li X, Wei K, Liang X. Study on preparing nanosized ITO powder by chemical liquid phase coprecipitation process. *Metal Mine*, 2008, 38(9): 73–77 (in Chinese)
32. Guo Y, Yang B, Xu B, Liu D, Feng T. Study on reagents and effecting factors in preparation process of indium tin oxide nanoparticles. *Materials Reports*, 2007, 21: 156–158 (in Chinese)
33. Huang J, Chen C, Huang Z, Fu J, Chen S, Jiang Y, Lu L, Xia Y, Zhao X. Preparation and growth mechanism of the flower-like whiskers of γ -, θ -, and α - Al_2O_3 phases by homogeneous precipitation/calcination method. *Ceramics International*, 2021, 47(12): 16943–16949
34. Zhang Y, Liu J. Hydrothermal preparation of cubic ITO powder and its photoelectric performance. *Chemical Journal of Chinese Universities*, 2017, 38(7): 1110–1116 (in Chinese)
35. Wang H, Xu X, Li X, Zhang J, Li C. Synthesis and sintering of indium tin oxide nanoparticles by citrate-nitrate combustion method. *Rare Metals*, 2010, 29(4): 355–360
36. Shan W, Wu L, Tao N, Chen Y, Guo D. Optimization method for green $\text{SrAl}_2\text{O}_4:\text{Eu}^{2+}$, Dy^{3+} phosphors synthesized via co-precipitation route assisted by microwave irradiation using orthogonal experimental design. *Ceramics International*, 2015, 41(10): 15034–15040
37. Zhu J, Chew D A S, Lv S, Wu W. Optimization method for building envelope design to minimize carbon emissions of building operational energy consumption using orthogonal experimental design (OED). *Habitat International*, 2013, 37: 148–154
38. Tan Y, Luo X, Mao M, Shu D, Shan W, Li G, Guo D. Optimization red emission of $\text{SrMoO}_4:\text{Eu}^{3+}$ via hydro-thermal co-precipitation synthesis using orthogonal experiment. *Current Applied Physics*, 2018, 18(11): 1403–1409
39. Hu X, Yang H, Guo T, Shu D, Shan W, Li G, Guo D. Preparation and properties of Eu and Dy co-doped strontium aluminate long afterglow nanomaterials. *Ceramics International*, 2018, 44(7): 7535–7544
40. Duan Y, Ye R, Yan X, Dai C, Tan J, Xu G. Effects of pH value and calcining temperature on indium tin oxide nanopowder synthesized by co-precipitation. *Materials Science and Engineering of Powder Metallurgy*, 2014, 19(3): 413–420 (in Chinese)
41. Kim S M, Seo K H, Lee J H, Kim J J, Lee H Y, Lee J S. Preparation and sintering of nanocrystalline ITO powders with different SnO_2 content. *Journal of the European Ceramic Society*, 2006, 26(1–2): 73–80
42. Tang A, Li X, Zhou Z, Ouyang J, Yang H. Mechanochemical synthesis of $\text{Ni}(\text{OH})_2$ and the decomposition to NiO nanoparticles: thermodynamic and optical spectra. *Journal of Alloys and Compounds*, 2014, 600: 204–209
43. Rakhshani M, Kamrannejad M M, Babaluo A A, Rezaei M, Aghjeh M R. Thermal degradation behavior and kinetic studies of polyacrylamide gel in TiO_2 nanoparticles synthesis. *Iranian Polymer Journal*, 2012, 21(12): 821–828
44. Li S Y, Lee C Y, Lin P, Tseng T Y. Low temperature synthesized Sn doped indium oxide nanowires. *Nanotechnology*, 2005, 16(4): 451–457
45. Jung J, Kim D H. Growth evolution of self-catalytic tin-doped indium oxide nanowires. *Journal of Alloys and Compounds*, 2020, 823: 153648
46. Lu J, Minami K, Takami S, Shibata M, Kaneko Y, Adschiri T. Supercritical hydrothermal synthesis and *in situ* organic modification of indium tin oxide nanoparticles using continuous-flow reaction system. *ACS Applied Materials & Interfaces*, 2012, 4(1): 351–354
47. Nguyen A K Q, Huynh T T, Ho V T T. Preparation and characterization of indium doped tin oxide (ITO) via a non-aqueous sol-gel. *Molecular Crystals and Liquid Crystals*, 2016, 635(1): 32–39
48. Kim K Y, Park S B. Preparation and property control of nanosized indium tin oxide particle. *Materials Chemistry and Physics*, 2004, 86(1): 210–221
49. Ray S, Banerjee R, Basu N, Batabyal A K, Barua A K. Properties of tin doped indium oxide thin films prepared by magnetron sputtering. *Journal of Applied Physics*, 1983, 54(6): 3497–3501
50. Fang X, Bando Y, Shen G, Ye C, Gautam U K, Costa P M F J, Zhi C, Tang C, Golberg D. Ultrafine ZnS nanobelts as field emitters. *Advanced Materials*, 2007, 19(18): 2593–2596

51. Walsh A, Da Silva J L F, Wei S H, Körber C, Klein A, Piper L F J, DeMasi A, Smith K E, Panaccione G, Torelli P, Payne D J, Bourlange A, Egdell R G. Nature of the band gap of In_2O_3 revealed by first-principles calculations and X-ray spectroscopy. *Physical Review Letters*, 2008, 100(16): 167402
52. Cuya Huaman J L, Tanoue K, Miyamura H, Matsumoto T, Jeyadevan B. Large-scale synthesis of ITO nanoparticles in an alcohol system assisted by acids. *New Journal of Chemistry*, 2014, 38(8): 3421–3428
53. Amin M, Ehsani N, Mozafarinia R. Effect of seeding and carbon content on the formation and microstructure of Ca- α -SiAlON. *International Journal of Refractory & Hard Metals*, 2019, 82: 208–214
54. Zhou S, Wang H, Zhong L, Li G. Synthesis and luminescence properties of cubic-shaped $\text{Ca}_{1-x}\text{TiO}_3:\text{Eu}^{3+}$ particles. *Luminescence*, 2018, 33(2): 443–449
55. Li S, Qiao X, Chen J, Wang H, Jia F, Qiu X. Effects of temperature on indium tin oxide particles synthesized by co-precipitation. *Journal of Crystal Growth*, 2006, 289(1): 151–156